

Measurement of the collisional self-broadening of the cesium $6S_{1/2} \rightarrow 5D_{3/2}$ (689-nm) electric quadrupole transition

A. Andalkar,* M. Iinuma,† J. W. Smit, and E. N. Fortson‡

Department of Physics, Box 351560, University of Washington, Seattle, Washington 98195-1560, USA

(Received 11 May 2004; published 11 November 2004)

We have measured the collisional self-broadening of the cesium $6S_{1/2} \rightarrow 5D_{3/2}$ electric quadrupole ($E2$) transition at 689 nm for temperatures from 220 to 370 °C, corresponding to cesium number densities from 3×10^{15} to 1.5×10^{17} cm $^{-3}$. This $E2$ transition may have utility for studies of atomic parity nonconservation (PNC), and the collisional self-broadening represents an important systematic effect which must be understood for an accurate measurement of PNC. We find a value for this broadening of $1.32 \pm 0.06 \times 10^{-8}$ cm 3 s $^{-1}$, which is consistent with what would be expected for a quadrupole-quadrupole resonance interaction. To the best of our knowledge, no quantitative measurement of the self-broadening of an atomic $E2$ transition has been reported previously in the literature.

DOI: 10.1103/PhysRevA.70.052703

PACS number(s): 34.20.-b, 32.70.Jz

I. INTRODUCTION

The recent high-precision measurement of parity nonconservation (PNC) on the $6S_{1/2} \rightarrow 7S_{1/2}$ transition in cesium [1] has spurred renewed interest in PNC measurements in cesium, both experimental and theoretical [2–5]. Several possible schemes for measuring PNC on other transitions in cesium have been proposed (see, e.g., Refs. [4,6]), including the $6S_{1/2} \rightarrow 5D_{3/2}$ electric quadrupole ($E2$) transition at 689 nm. We have measured the collisional self-broadening of this $E2$ transition at temperatures from 220 to 370 °C, corresponding to cesium number densities from 3×10^{15} to 1.5×10^{17} cm $^{-3}$. This covers the range of Cs number densities expected to be of use in a PNC experiment, where the self-broadening represents an important systematic effect on the line shape which must be understood for an accurate measurement.

The $6S_{1/2} \rightarrow 5D_{3/2,5/2}$ quadrupole transitions (see Fig. 1) in cesium have been studied several times previously. Most measurements date from the 1970s, when several studies measured the oscillator strengths [7–9] of these transitions and the hyperfine structure of the $5D_{3/2,5/2}$ states [10]. More recent studies of these states have measured the lifetimes [11–13] and hyperfine structure [14]. Since the $E2$ transitions are quite weak, with oscillator strengths in the 10^{-7} range, collisional self-broadening becomes an important effect at the high number densities (roughly 10^{15} – 10^{17} cm $^{-3}$ needed to produce sufficient absorption for experimental work. However, only two previous studies [7,9] have investigated this broadening, both quite briefly and semiquantitatively.

Several measurements have been made of the collisional self-broadening of electric dipole ($E1$) transitions, for ex-

ample the cesium $6S_{1/2} \rightarrow 6P_{1/2,3/2}$ ($D1$ and $D2$) transitions (see, e.g., Refs. [15–18]). To the best of our knowledge, such measurements on $E2$ transitions in atoms have not been reported previously in the literature. The strong dipole-dipole resonance broadening on the $D1$ and $D2$ lines is qualitatively and quantitatively different from the broadening of the 689 nm $E2$ line, where the quadrupole-quadrupole resonance interactions are very weak and are comparable with the nonresonant collisional broadening (pressure broadening). The interaction strength for dipole-dipole interactions varies with distance as $V(R) \propto R^{-3}$, while it goes as R^{-5} for quadrupole-quadrupole interactions and R^{-6} for nonresonant (van der Waals) interactions such as those with a foreign gas [19]. Thus we would expect the value of the 689 nm self-broadening to be considerably less than the self-broadening of an electric-dipole allowed transition such as the $D1$ or $D2$, yet somewhat larger than the collisional broadening of cesium transitions due to typical foreign gases.

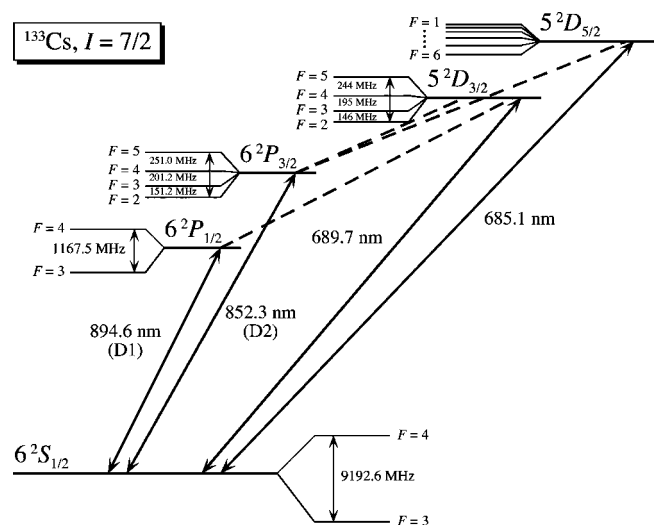


FIG. 1. The lowest energy levels and transitions in cesium, including the 689 nm and 852 nm lines of primary interest in this work. Dashed lines show the electric-dipole allowed transitions out of the $5D$ states. Hyperfine splittings are also shown for each state.

*Electronic address: andalkar@u.washington.edu

†Present address: Graduate School of Advanced Sciences of Matter, Hiroshima University, 1-3-1 Kagami-Yama, Higashi-Hiroshima 739-8526, Japan.

‡Electronic address: fortson@phys.washington.edu; URL: <http://www.phys.washington.edu/~fortson/>

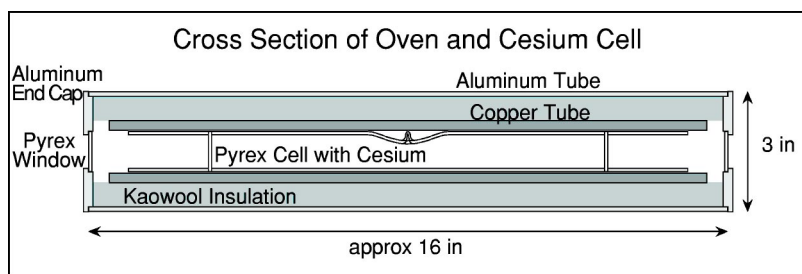
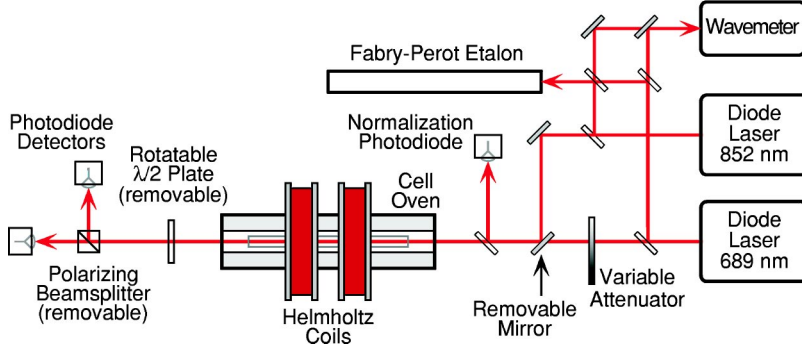


FIG. 2. (Color online) Diagram of the experimental apparatus, with an inset showing details of the oven and cesium cell.



II. EXPERIMENTAL APPARATUS AND METHOD

A diagram of the experimental apparatus is shown in Fig. 2. The basic method used here to measure the collisional self-broadening involves fitting a Voigt profile line shape to an absorption spectrum in a heated cesium vapor cell. The frequency of a tunable diode laser at 689 nm is scanned across the $6S_{1/2} \rightarrow 5D_{3/2}$ hyperfine spectrum, and the Lorentzian width is extracted from the fit. This simple experimental technique works well on the weak 689 nm transition, since the absorption is typically only a few optical depths at number densities for which the collisional broadening becomes large enough to be extracted accurately from the Doppler-broadened line shape. For strong transitions such as the Cs $D1$ or $D2$ lines, more sophisticated techniques such as Doppler-free spectroscopy are required.

The cesium number density is obtained from the fitted absorption strength on the 689 nm transition and also independently calibrated by Faraday rotation in the wings of the 852 nm $D2$ transition. An important experimental consideration here is that the line-shape fitting technique works best for scans which have roughly between 0.5 and 3 optical depths on the peaks of the absorption profile. In order to take data over a large range of cesium density (about two orders of magnitude), it is necessary to vary the optical path length through the vapor, either by using cells of different lengths or by a more complicated multiple-pass arrangement with a single cell. We chose the simpler method, and designed the oven to allow a simple interchange of cells of several lengths. The oven is also designed to maintain a temperature uniformity of better than 1°C over a 12-in.-long by 1-in.-diam cylindrical region, which limits variation in the Doppler width (Δ) over the cell to less than 1 part in a 1000 (since $\Delta \propto \sqrt{T}$ and $T > 500\text{ K}$ for these measurements). Uncontrolled variation would cause a serious systematic effect in the line-shape fitting, and this level of temperature uniformity reduces such effects to an insignificant amount.

The oven consists of a 15-in.-long thick-wall copper tube (1.5-in. outer diameter by 0.250-in. wall), spiral-wrapped with a single layer of 0.5-in.-wide, double-insulated Samox heater tape (Omega STH151-080), and surrounded by a 0.75-in.-thick blanket of Kaowool fiber insulation. Inside the heater tape are four thermocouples, resting in shallow slots sawed partway into the wall of the copper tube, which are spaced over the length of the tube to allow measuring the temperature uniformity. This entire assembly is placed inside a 16-in.-long aluminum tube (3.0-in. outer diameter by 0.125-in. wall), which is cut lengthwise into a clamshell arrangement for ease of assembly. The ends of the tube are closed with aluminum endcaps 0.25 in. thick with 1-in.-diam Pyrex windows for optical access, and the clamshell and endcaps are clamped solidly together using twist-ties made of 18 AWG copper wire. A digital temperature controller with fuzzy logic (Omega CN4431) controls the current to the heater tape through a solid-state relay (Omega SSR330DC25), using the central thermocouple as its temperature sensor. This control system has an observed stability of better than 0.2°C , and when the temperature setpoint is changed, the fuzzy logic controller provides rapid restabilization, much faster than the natural thermal relaxation time of the oven.

The cells are also designed to maximize temperature uniformity over their length and to present a nearly identical thermal load to the oven while providing differing optical path lengths. The three cells used for the measurements consist of cylindrical Pyrex tubes, 1 in. diam and nominally 1 in., 2 in., and 10 in. in length, with planar windows fused on the ends and 1-in.-diam cylindrical extensions fused on to each end window to bring the total length of each cell to 14 in.. The active optical path lengths are 2.3 cm, 4.7 cm, and 25.2 cm. The cells are baked and evacuated to roughly 10^{-7} torr, and a small droplet of 99.98% pure Cs metal is distilled into each prior to sealing off. The tubulation on each cell is recessed within a depression where it joins the side

wall, so that after seal-off, the stem that remains does not protrude beyond the nominal 1 in. diam of the cell (see Fig. 2 inset).

Several thin thermocouples are attached to the outside of each cell (six on the longest cell and four on the others) to monitor temperature uniformity along the cell itself, and are held in place by glass cloth electrical tape (Scotch 27) which maintains adhesion even at temperatures far beyond its 130 °C rating. The measured temperature uniformity is better than 1 °C over the length of the cell, but as expected the coldest portion of the cells is at the centers of the end windows. Over extended periods of time (hours) at high temperatures, the cesium metal would tend to migrate and condense on the windows, impeding optical access. To solve this problem, single loops of nichrome heater wire are wrapped around the cell at the location of each end window, and a 1 A current is run through the wire. This maintains the window at a slightly higher temperature to prevent cesium deposition, while still maintaining uniformity better than 1 °C.

Surrounding the middle of the oven assembly are a pair of Helmholtz coils, which provide a field of 300 G with a uniformity better than 1 G over a 6-cm-long by 2-cm-diam cylindrical region, which covers the volume of the two shorter cells. (The additional field due to the nichrome loops mentioned above is less than 0.5 G.) An attempt was initially made to build an end-compensated solenoid which could provide a similar magnitude and uniformity of field over the larger volume of the 25-cm-long cell, but this was difficult to achieve with reasonable effort and so it was abandoned in favor of the Helmholtz pair. Therefore, Faraday rotation data could only be acquired for the two shorter cells, but this was not a major limitation since the broadening data in the longer cell was of marginal quality anyway (see Sec. III).

The two external-cavity diode lasers are a lab-built 689 nm system and a commercial New Focus 6226 system at 852 nm. The 689 nm system uses a very simple cavity design consisting of two high-precision kinematic mounts (Lees LM1) holding the diffraction grating and the collimating lens, with the diode (Hitachi HL6738MG) secured onto the fixed portion of the lens mount. Single-mode power output for this system is about 10 mW at 689 nm, with a linewidth of a few MHz and a continuous scanning range of over 15 GHz.

A Melles Griot SuperBand optical spectrum analyzer, consisting of a scanning confocal Fabry-Perot etalon with a free spectral range (FSR) of 300 MHz, provided confirmation that each diode laser was operating in a single longitudinal mode. With its piezo scan halted, the etalon was used to provide marker fringes as the laser frequency was scanned during each line-shape measurement. This allowed determination and correction of any nonlinearity in the frequency scan as detailed in Sec. III. The fringes were broadened by degrading the finesse of the etalon, using one mirror outside its intended wavelength range to give a finesse of roughly 20. This serves to eliminate aliasing effects caused by undersampling due to the limited number of data points in each scan.

III. COLLISIONAL BROADENING DATA AND FITTING PROCEDURE

The data acquisition system consists of a computer and 16-bit data acquisition board. A pair of 12-bit digital-to-

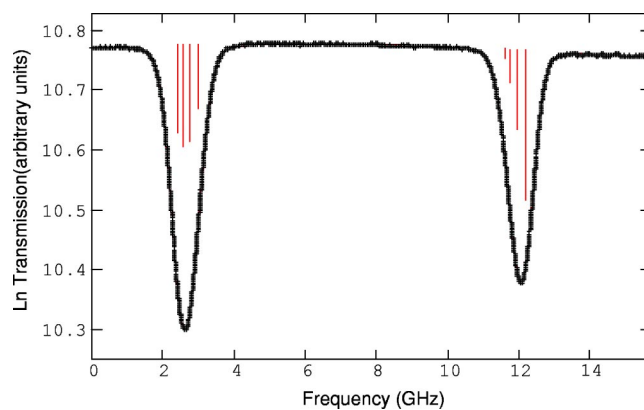


FIG. 3. (Color online) Typical collisional broadening scan across the 689 nm hyperfine spectrum, in this example using the 2.3 cm cell at 310 °C, showing both data and fit (the fitted curve is hidden by the data). The centers and relative magnitudes of the fitted hyperfine components are shown by the lines within each peak.

analog converter (DAC) outputs is used to scan the 689 nm laser across the transition by simultaneously varying the grating angle and laser current in opposite senses, thus achieving typical scan widths of about 15 GHz. Data are simultaneously acquired for the cell transmission, intensity normalization, and etalon marker fringes, with 4096 data points taken in each scan.

In order to extract the values of the pressure broadening and shift, a Voigt profile which includes the appropriate hyperfine components is fit to each absorption spectrum. A custom-written line-shape-fitting program performs a general nonlinear least-squares fit of a Voigt profile (Fig. 3). Fixed parameters in the fitting function include the ground- and excited-state hyperfine splittings (taken from the most recent measurements in Ref. [14]), along with the calculated relative strengths of each hyperfine component. For all fits presented here, the Doppler width is held as a fixed parameter and set to the calculated value for the measured temperature, $\Delta = 4\pi\lambda^{-1}\sqrt{2(\ln 2)kT/M}$, with values of about 600–680 MHz at $\lambda = 689$ nm over the temperature range from 220 to 370 °C. The steps taken to ensure temperature uniformity over the entire cell (see Sec. II) justify holding the Doppler width fixed.

Free parameters consist of the Lorentzian width Γ [full width at half-maximum (FWHM)], total scan range, frequency offset, and integrated optical depth A , along with four parameters to define a third-order polynomial background on which the absorption peaks lie, to account for uncanceled background variation. Note that the frequency offset as defined here is the distance from the start of a scan to the center of the hyperfine spectrum. The value of A should equal $nL\sigma_0$, where n is the number density, L is the path length, and $\sigma_0 = \int \sigma(\nu) d\nu = \pi r_e f$ is the integral of the absorption cross section with r_e the classical electron radius and f the oscillator strength of the relevant transition. Thus the fitted value of A provides a good cross-check on the quality of the fits as the temperatures increase and the linewidths broaden.

Prior to fitting the line shape, the frequency axis is linearized using the marker fringes from the Fabry-Perot etalon.

For broad fringes at low finesse, it is sufficient to do a five-point quadratic fit on each peak to extract the position of its center. Once this is done, a cubic fit to the fringe positions gives the nonlinearity of the frequency scale, since the fringes are spaced at equal intervals of the etalon FSR of 300 MHz.

Line-shape data were acquired over a broad range of temperatures in each of the three cells used, 220–300 °C in the 25.2 cm cell, 250–360 °C in the 4.7 cm cell, and 260–370 °C in the 2.3 cm cell. All of the data from the longest cell were of limited utility, since the collisional broadening was quite small relative to the large Doppler width over the useful range of optical depths. The data at lower temperatures in the two shorter cells also suffered from a small collisional broadening of order 10 MHz, which is difficult to extract accurately from the much larger Doppler width. The upper end of the usable temperature range was limited by the increasing likelihood of the cesium attacking the Pyrex cell, which becomes significant above 350 °C.

Data sets were acquired at 5 °C increments in each cell. After increasing the temperature, a waiting period of about 10 min allowed the oven and cell to reach thermal equilibrium. Five line-shape scans were then taken, each requiring about 1 min to scan across the 15 GHz range, and then the temperature was increased again. To test for any hysteresis effects due to the cell failing to reach thermal equilibrium, data on the long cell were also acquired in the same manner while decreasing the temperature. No such effects were discernible, as the fitted linewidths were statistically identical at the same temperature for both directions of temperature change.

The broadening coefficient $\kappa = \Gamma/n$ is expressed as a ratio of the Lorentzian width Γ to the number density n in the cell, and in order to calculate it we simply make a linear fit to the values of Γ as a function of n . Note that the Lorentzian width Γ includes not only the collisional broadening of interest, but also the natural linewidth and the laser linewidth. However, the latter two make a negligible contribution and are ignored here. The lifetime of the $5D_{3/2}$ state is about 900 ns [11] dominated by decay via the $6P_{1/2,3/2}$ states, corresponding to a natural linewidth of about 180 kHz, and the linewidth of our 689 nm laser is about 1–2 MHz, while the total Lorentzian widths exceed 300 MHz at the upper end of the temperature range investigated here.

IV. MEASUREMENT OF CESIUM NUMBER DENSITY

After the data sets are fit to extract the Lorentzian width, the next step in the data analysis is to convert the temperature values into cesium number density. The usual method for doing so is to use a formula from one of the standard vapor pressure references (see, e.g., Refs. [21–23]). However, an additional complication arises here because the Cs vapor pressure in a glass cell is typically somewhat less than the vapor pressure above a free surface of liquid Cs would be, due to the interactions of the strongly reactive Cs atoms with the walls of the cell which become increasingly significant at higher temperatures. In any case, the values obtained

from vapor pressure equations for Cs in these references have a stated accuracy only at the several percent level over the temperature range of interest here. In order to achieve greater accuracy, we measure the Cs number density in the cell directly, using both the absorption on the 689 nm line itself and also Faraday rotation of plane-polarized light on the much stronger 852 nm $D2$ transition. Together, these measurements provide a much improved and more precise calibration of the broadening versus number density.

The standard method for determining the number density of an atomic vapor involves measuring the absorption of light near an atomic transition, then calculating the number density using the known oscillator strength. However, for the 689 nm transition, the oscillator strength f is known only with a precision of about 5%. The most recent measurement made over two decades ago found that $f = 3.28 \pm 0.16 \times 10^{-7}$ [9], which was fairly consistent with earlier measurements in Refs. [7,8]. Thus our calculation of the number density in the cell using the fitted value of the integrated optical depth $A = nL\pi c r_e f$ for each data point is limited by the accuracy in the available value for f . Further improving the accuracy requires using a different transition for which the value of f is more precisely known.

Along with the issue of accuracy, there is the important caveat that the fitted value for A is not completely independent of the fitted value of the Lorentzian width Γ . In a non-linear least-squares fit to a Voigt profile, there is always some degree of inverse correlation between the fitted values for these two parameters. Thus using A to determine the number density n could possibly introduce an undesirable systematic effect into the linear fit used to calculate the broadening coefficient κ . Therefore, an additional benefit of using a separate transition to measure the number density is that this possible source of systematic correlation can be eliminated.

In contrast with the 689 nm line, the oscillator strengths for the $D1$ and $D2$ transitions are known to about 0.3%. Recent lifetime measurements of the $6P_{1/2,3/2}$ states by two different methods [24,25] each have an accuracy of better than 0.3%, and the absolute frequencies of the $D1$ and $D2$ lines have been measured to better than 1 part in 10^9 [26,27], combining to give values for the oscillator strengths of 0.3421 ± 0.0010 on the $D1$ and 0.7125 ± 0.0016 on the $D2$. However, with oscillator strengths of order unity, the absorption on these electric-dipole allowed transitions is far too strong at the temperatures of interest here, producing millions of optical depths in our cells near line center. Thus we require a technique which uses the wings of these lines, and so it is best to use Faraday rotation instead of absorption, since the rotation falls off inversely with the square of the frequency detuning from line center while the absorption falls off exponentially for a primarily Doppler-broadened line.

The use of Faraday rotation for measuring the number density and polarization of alkali-metal vapors has become an increasingly standard technique over the past two decades [28–30]. Our method here follows closely that of Ref. [30]. We use an 852 nm tunable diode laser to measure the Faraday rotation over a range of about 15 nm centered on the $D2$ transition ($6S_{1/2} \rightarrow 6P_{3/2}$), as shown in Fig. 4. A Burleigh WA-1500 wavemeter provides the wavelength measurement,

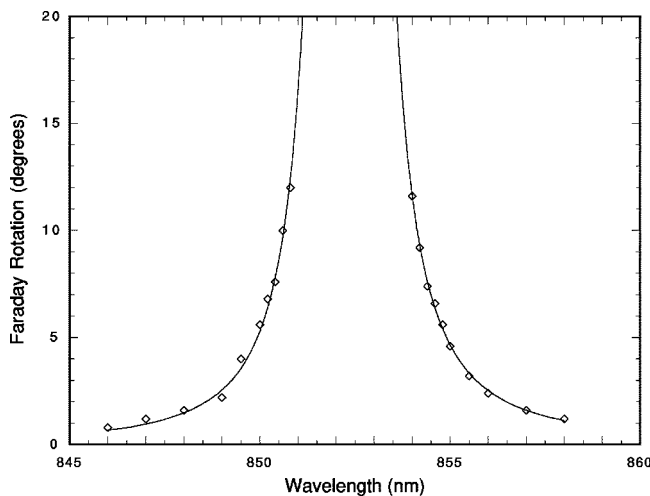


FIG. 4. Typical Faraday rotation data on the 852 nm $D2$ line, using the 2.3 cm cell at 290 °C with a field of 300 G. The fitted curve includes all three significant terms (symmetric, antisymmetric, and paramagnetic).

with an absolute accuracy better than 0.01 nm, and the angle is read from a vernier scale on the rotation stage holding the half-wave plate, with an accuracy of about 0.1 deg. The uniform magnetic field of 300 G is produced by the Helmholtz coils mentioned earlier in Sec. II. Data were taken over the range of 210–320 °C, in 10 °C increments for both directions of magnetic field. Above 320 °C, the dark region near line center becomes too broad for accurate measurements, as the vapor is essentially opaque over greater than a 5 nm range while the scanning range of the aging New Focus 6226 laser was limited to less than 15 nm.

To fit the rotation data and extract the number density, the proper functional form of the Faraday rotation must be known. For large detunings, the hyperfine structure can be ignored and the Faraday rotation can be expressed quite simply as the sum of three major terms, namely symmetric, antisymmetric, and paramagnetic,

$$\theta(\lambda) = nLr_e\lambda \frac{\mu_B B}{h} \left[\frac{\lambda}{2c} \left(\frac{4}{3} \frac{f_1 \lambda_1}{(\lambda - \lambda_1)^2} + \frac{7}{6} \frac{f_2 \lambda_2}{(\lambda - \lambda_2)^2} \right) + \frac{\lambda_1 \lambda_2}{9c(\lambda_1 - \lambda_2)} \left(\frac{\lambda_2}{\lambda - \lambda_2} - \frac{\lambda_1}{\lambda - \lambda_1} \right) \pm \frac{1}{6} \frac{h}{kT} \left(\frac{\lambda_1}{\lambda - \lambda_1} - \frac{\lambda_2}{\lambda - \lambda_2} \right) \right], \quad (1)$$

where n is the number density, L the path length, r_e the classical electron radius, f_1 and f_2 the oscillator strengths of the $D1$ and $D2$ transitions, and λ_1 and λ_2 the wavelengths of these transitions. The symmetric term is by far the largest for the case at hand, with the other two terms contributing at the few percent level for unpolarized cesium atoms. The antisymmetric term which arises due to state mixing has a small but significant contribution in cesium. The paramagnetic term is also antisymmetric about each fine-structure component and changes sign relative to the other two terms upon magnetic field reversal, with its magnitude depending on the degree of atomic spin polarization.

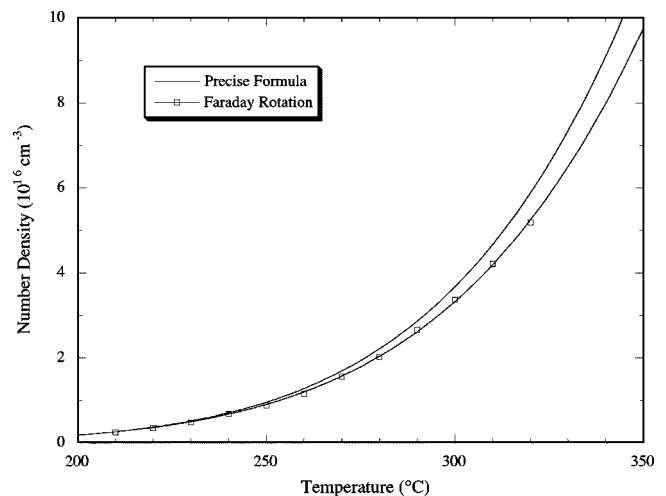


FIG. 5. Comparison of Cs number density calculated using the “precise” formula from Ref. [23] with that obtained from the Faraday rotation data. A curve of the same functional form has been fit to the Faraday data.

We fit a standard vapor pressure equation of the form $\log p = A + B/T + C \log T$ to the Faraday rotation data to derive values for the coefficients. Our fitted equation is $\log p(\text{atm}) = 8.091 - 3956/T - 1.3677 \log T$, versus the “precise” formula from Ref. [23] of $\log p(\text{atm}) = 8.232 - 4062/T - 1.3359 \log T$. A comparison of the number density calculated using the formula with that obtained from our Faraday rotation data is shown in Fig. 5. The standard formula is higher than our measured number density by roughly 2% at 210 °C, increasing to 14% at 370 °C. This growing divergence is attributable to the larger interactions of the Cs atoms with the cell walls at higher temperatures, and demonstrates the need for an actual measurement of the number density.

V. RESULTS

Our results for the collisional broadening are shown in Fig. 6 and Table I. The values for the broadening κ are calculated by making one-parameter straight-line fits (constrained to pass through zero) to the measured Lorentzian widths as a function of the cesium number density in the cell, as calculated from both the absorption on the 689 nm transition and the Faraday rotation on the 852 nm transition. Note that only data from the two shorter cells have been used here in the final analysis, since as mentioned earlier in Sec. III, the data from the longest cell suffered from having a very small collisional broadening over its useful range of optical depths. Also, the major source of systematic uncertainty in this experiment is the determination of the number density, and this was also most suspect in the longest cell, for which Faraday rotation data could not be acquired. The excellent agreement between the number densities (and thus the values for the broadening coefficients κ) for the two shorter cells calculated using these two complementary but very dissimilar methods is strong evidence that the density has been accurately measured, and that the uncertainties are limited to the few percent level. The weighted mean of the four slopes in Table I is $\kappa = 2.098 \pm 0.089 \times 10^{-9} \text{ cm}^3 \text{ Hz}$, where the overall error is

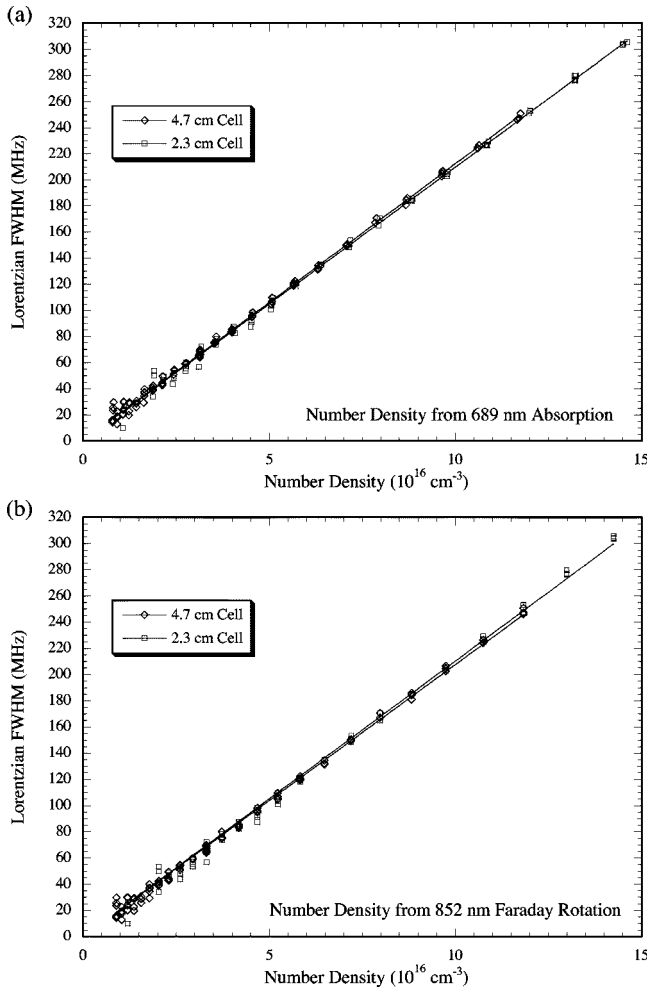


FIG. 6. Results for the collisional broadening, plotted vs the number density derived from (a) absorption on the 689 nm transition, and (b) Faraday rotation on the 852 nm transition. Straight line fits are shown through the data points, and the error bars on each point are smaller than the markers.

the RMS of the total errors on the individual slopes (shown in the final column of Table I). The standard deviation in the values of the four slopes about the mean is $0.017 \times 10^{-9} \text{ cm}^3 \text{ Hz}$, significantly less than the overall error bar. Our final number for the collisional self-broadening of the cesium 689 nm $E2$ transition is this weighted mean value, $\kappa = 2.10 \pm 0.09 \times 10^{-9} \text{ cm}^3 \text{ Hz}$, which can be converted to the more standard units as $\kappa = 1.32 \pm 0.06 \times 10^{-8} \text{ cm}^3 \text{ s}^{-1}$.

A brief explanation of the uncertainties (errors) shown in Table I follows. The linear error is simply the error on the

slope of these linear fits. However, the Voigt error and density error are more complicated. The vertical error bars on each point in Fig. 6 come from the error in the fitted value of the Lorentzian width as given by the nonlinear least-squares fitting program. These calculated error bars are about 2–4 % for the smallest widths (under 20 MHz), decreasing to less than 1% for widths above 40 MHz and to only 0.1–0.2 % for the largest widths above 100 MHz. The data points for the smaller widths have little bearing on the slope of the one-parameter straight-line fit, which is constrained to pass through zero. The slope and the uncertainty in that value are determined primarily by the more robustly fitted data points for widths above 100 MHz. The calculation of the fitting error assumes purely statistical behavior of the data (i.e., that measurement errors are independent from point to point and normally distributed), which does not strictly hold for these data sets, and so the actual uncertainties may be somewhat larger than the values calculated by the fitting program. Thus the Voigt error listed here is 1% of the slope, to account for the nonstatistical behavior and to provide a conservative estimate of the errors.

For the fits using 689 nm absorption to determine number density, the density error is dominated by the uncertainty in the value of the oscillator strength f , which is about 5% [9]. For the fits using Faraday rotation, the value of the density error for each point comes primarily from the Faraday fit errors for the functional form shown in Fig. 4. These errors range from about 0.5% below 250 °C up to about 2% at 320 °C. Since values above this temperature have been extrapolated, the density errors are likely to be even higher for the upper end of the range. Thus the density error is assumed to be about 3% for these fits, again to provide a conservative estimate of the errors. In both cases, the density error provides the dominant contribution to the total error, which is simply the sum in quadrature of the linear, Voigt, and density errors.

A possible additional source of systematic error in the experiment is the presence of Cs_2 molecules, which are a known limitation for cell-based cesium PNC experiments (see, e.g., Refs. [2,31]). The relative abundance of Cs_2 dimers in chemical equilibrium with the Cs atoms increases from about 0.3% at 220 °C to over 2% at 370 °C, based on the chemical equilibrium coefficients calculated in Ref. [32]. We assume that the atomic Cs number density as measured here by the 689 nm absorption and 852 nm Faraday rotation reflects the true density of Cs atoms in the cell, while the Cs_2 molecules behave as a separate chemical species in equilibrium with both the atomic vapor and the liquid cesium drop-

TABLE I. Slopes and errors for the linear fits shown in Fig. 6, in units of $10^{-9} \text{ cm}^3 \text{ Hz}$. See the text for an explanation of the listed error values.

Number density	Cell length	Slope κ	Linear error	Voigt error	Density error	Total error
689 Absorption	2.3 cm	2.098	0.005	0.021	0.105	0.107
689 Absorption	4.7 cm	2.124	0.005	0.021	0.106	0.108
852 Faraday	2.3 cm	2.104	0.008	0.021	0.063	0.067
852 Faraday	4.7 cm	2.077	0.006	0.021	0.062	0.066

lets. Although the Cs_2 molecules do not contribute to the quadrupole-quadrupole resonance broadening, they would cause some collisional broadening as a foreign gas due to van der Waals interactions. Since the Cs_2 molecular number density is less than 3% that of Cs atoms at our highest temperature and the van der Waals interactions are somewhat weaker than the quadrupole-quadrupole interactions, it is likely that this source of systematic error contributes at less than the 1% level.

VI. CONCLUSION

We have measured the collisional self-broadening of the cesium $6S_{1/2} \rightarrow 5D_{3/2}$ electric quadrupole ($E2$) transition at 689 nm for temperatures from 220 to 370 °C, corresponding to cesium number densities from 3×10^{15} to $1.5 \times 10^{17} \text{ cm}^{-3}$. We find a value for this self-broadening of $\kappa = 1.32 \pm 0.06 \times 10^{-8} \text{ cm}^3 \text{ s}^{-1}$, with an overall uncertainty of better than 5%. The measured 689 nm self-broadening is roughly a factor of 50 smaller than the self-broadening on the Cs $D1$ or $D2$ transitions ($\kappa_{D1} = 5.7 \pm 1.0 \times 10^{-7} \text{ cm}^3 \text{ s}^{-1}$ and $\kappa_{D2} = 6.7 \pm 1.1 \times 10^{-7} \text{ cm}^3 \text{ s}^{-1}$ based on the latest avail-

able values in Ref. [17]). It is also roughly a factor of 3 larger than the broadening of the Cs $D1$ and $D2$ lines by foreign gases such as N_2 or He, which have typical values of about $4 \times 10^{-9} \text{ cm}^3 \text{ s}^{-1}$ [20]. Our results are thus consistent with what would be expected from the relative strength of a quadrupole-quadrupole resonance interaction. The van der Waals interactions among the cesium atoms may also be contributing significantly to the measured broadening, perhaps at the 20–30 % level assuming that they behave similarly to a foreign gas. However, these interactions could be contributing an even larger share of the total broadening, since cesium itself is more easily polarizable than foreign gases such as N_2 or He and thus would have larger induced interatomic forces. Detailed calculations and more detailed measurements of the line shapes could perhaps quantify these contributions.

ACKNOWLEDGMENTS

We thank R. Bruce Warrington for the development of our Voigt line-shape fitting program and Rob Lyman for assistance with the data analysis. This project is supported by the National Science Foundation under Grant No. PHY-0099535.

-
- [1] C. S. Wood, S. C. Bennett, D. Cho, B. P. Masterson, J. L. Roberts, C. E. Tanner, and C. E. Wieman, *Science* **275**, 1759 (1997).
- [2] M.-A. Bouchiat and C. Bouchiat, *Rep. Prog. Phys.* **60**, 1351 (1997).
- [3] W. R. Johnson, in *Proceedings of the 18th International Conference on Atomic Physics* (2003), Vol. 66, pp. 327–337.
- [4] V. A. Dzuba, V. V. Flambaum, and J. S. M. Ginges, *Phys. Rev. A* **63**, 062101 (2001).
- [5] V. A. Dzuba, V. V. Flambaum, and J. S. M. Ginges, *Phys. Rev. D* **66**, 076013 (2002).
- [6] A. D. Cronin, Ph.D. thesis, University of Washington (1999).
- [7] B. Sayer, R. Wang, J. C. Jeannet, and M. Sassi, *J. Phys. B* **4**, L20 (1971).
- [8] R. J. Exton, *J. Quant. Spectrosc. Radiat. Transf.* **16**, 309 (1976).
- [9] K. Niemax, *J. Quant. Spectrosc. Radiat. Transf.* **17**, 125 (1977).
- [10] K. Fredriksson, H. Lundberg, and S. Svanberg, *Phys. Rev. A* **21**, 241 (1980).
- [11] D. DiBerardino, C. E. Tanner, and A. Sieradzan, *Phys. Rev. A* **57**, 4204 (1998).
- [12] A. Sasso, W. Demtröder, T. Colbert, C. Wang, E. Ehrlacher, and J. Huennekens, *Phys. Rev. A* **45**, 1670 (1992).
- [13] B. Hoeling, J. R. Yeh, T. Takekoshi, and R. J. Knize, *Opt. Lett.* **21**, 77 (1996).
- [14] W. Yei, A. Sieradzan, E. Cerasuolo, and M. D. Havey, *Phys. Rev. A* **57**, 3419 (1998).
- [15] C. Gregory, *Phys. Rev.* **61**, 465 (1942).
- [16] C. L. Chen and A. V. Phelps, *Phys. Rev.* **173**, 62 (1968).
- [17] Z. J. Jabbour, J. Sagle, R. M. Namiotka, and J. Huennekens, *J. Quant. Spectrosc. Radiat. Transf.* **54**, 767 (1995).
- [18] V. Vuletić, V. A. Sautenkov, C. Zimmerman, and T. W. Hänsch, *Opt. Commun.* **99**, 185 (1993).
- [19] I. I. Sobelman, L. A. Vainshtein, and E. A. Yukov, *Excitation of Atoms and Broadening of Spectral Lines*, 2nd ed. (Springer-Verlag, Berlin, 1995).
- [20] A. Andalkar and R. B. Warrington, *Phys. Rev. A* **65**, 032708 (2002).
- [21] J. B. Taylor and I. Langmuir, *Phys. Rev.* **51**, 753 (1937).
- [22] A. N. Nesmeyanov, *Vapour Pressure of the Elements* (Academic Press, New York, 1963).
- [23] C. B. Alcock, V. P. Itkin, and M. K. Horrigan, *Can. Metall. Q.* **23**, 309 (1984).
- [24] L. Young, W. T. Hill III, S. J. Sibener, S. D. Price, C. E. Tanner, C. E. Wieman, and S. R. Leone, *Phys. Rev. A* **50**, 2174 (1994).
- [25] R. J. Rafac, C. E. Tanner, A. E. Livingston, and H. G. Berry, *Phys. Rev. A* **60**, 3648 (1999).
- [26] T. Udem, J. Reichert, R. Holzwarth, and T. W. Hänsch, *Phys. Rev. Lett.* **82**, 3568 (1999).
- [27] T. Udem, J. Reichert, T. W. Hänsch, and M. Kourogi, *Phys. Rev. A* **62**, 031801(R) (2000).
- [28] Z. Wu, M. Kitano, W. Happer, M. Hou, and J. Daniels, *Appl. Opt.* **25**, 4483 (1986).
- [29] J. Stenger, M. Beckmann, W. Nagengast, and K. Rith, *Nucl. Instrum. Methods Phys. Res. A* **384**, 333 (1997).
- [30] E. Vliegen, S. Kadlacek, L. W. Anderson, T. G. Walker, C. J. Erickson, and W. Happer, *Nucl. Instrum. Methods Phys. Res. A* **460**, 444 (2001).
- [31] M. Lintz and M. A. Bouchiat, *Phys. Rev. Lett.* **80**, 2570 (1998).
- [32] C. J. Erickson, Ph.D. thesis, Princeton University, 2000; see Chap. 6.